Available online at www.sciencedirect.com
ScienceDirect
Journal of Power Sources 179 (2008) 17–26
JOURNAL OF POWER SOURCES
www.elsevier.com/locate/jpowsour

Electrocatalysis by nanocrystalline tungsten carbides and the effects of codeposited silver

C.D.A. Brady, E.J. Rees, G.T. Burstein *

Department of Materials Science and Metallurgy, University of Cambridge, Pembroke Street, Cambridge CB2 3QZ, United Kingdom

Received 15 November 2007; received in revised form 21 December 2007; accepted 1 January 2008
Available online 4 January 2008

Abstract

The electrocatalytic activity of two nanocrystalline tungsten carbides, WC and W_2C, towards the anodic oxidation of hydrogen in 1.5 M H_2SO_4 at 65 °C is presented. The carbides, which were synthesised by solid-state reduction of W(VI) using carbon, are both electrocatalytic. The WC phase shows greater electrocatalysis than the W_2C phase, and also shows a greater degree of passivity against corrosion in the hot sulphuric acid electrolytes. The effect of codeposited silver is to enhance the electrocatalytic activity of the WC phase, whilst not in itself showing any electrocatalysis.

Keywords: Tungsten carbide; Electrocatalysis; Passivity; Hydrogen oxidation; Base electrocatalyst

1. Introduction

Fuel cells offer potentially efficient, silent and low-pollution electrical power generation. Technical and economic problems have however, restricted their widespread development to just specialist niche markets. One of the principal factors hampering the extensive commercialisation of low-temperature acidic fuel cells is their dependence on the platinum group metals (PGM) as electrocatalysts. Platinum is expensive and large-scale commercialisation of fuel cells dependent on platinum is economically unattractive. Platinum is also susceptible to poisoning by carbon monoxide [1] and performance degradation with time at low electrode loadings [2]. Research into the production of electrocatalysts made from non-noble metals for low-temperature acidic electrolytes is therefore a highly applicable and potentially rewarding field of enquiry.

Tungsten carbide has been suggested previously for potential anode electrocatalyst [3,4]. It is a low-cost material that does not poison significantly in the presence of CO [5]. It is used as an abrasive [6]. Nickel tungsten carbides also show hydrogen oxidation catalysis [7] and methanol electrocatalysis [8–10]. Sputtered nickel tantalum carbide has shown electrocatalytic activity as both an anode and cathode [11]. Iron, cobalt and nickel-based porphyrins [12,13] have shown some electrocatalysis towards oxygen reduction and molybdenum nitride [14] and tungsten nitride [15] have been suggested as a possible alternative cathode electrocatalysts.

Three fundamental material properties must be satisfied for a base electrocatalyst. The material must be electronically conductive. It must be suitably stable in the electrolyte of choice which implies a high degree of passivity against corrosion, particularly in acidic electrolytes. It must also have high electrocatalytic activity for the desired reaction. Both tungsten carbides, WC and W_2C are good electronic conductors [16]. Non-noble metal catalysts must passivate within the fuel cell environment to maintain a corrosion rate low enough for an appropriate electrode lifetime. Tungsten is known to form a passivating oxide film in acidic solution at low potentials but corrodes at higher potentials [17]. Tungsten carbide shows similar passive behaviour in hot sulphuric acid. Silver additions to electrode materials have been shown to improve electrocatalytic performance [18,19]. This paper reports the passivation and electrocatalytic properties of nanocrystalline tungsten carbide with stoichiometries WC and W_2C synthesised via a solid-state thermal reduc-

* Corresponding author. Tel.: +44 1223 334361; fax: +44 1223 334567.
E-mail address: gtb1000@cam.ac.uk (G.T. Burstein).

0378-7753/$ – see front matter © 2008 Elsevier B.V. All rights reserved.
doi:10.1016/j.jpowsour.2008.01.002

tion reaction. We also report the effects of silver additions to WC on electrocatalytic hydrogen oxidation and reduction of H^+.

2. Experimental

2.1. Electrocatalyst synthesis

Nanocrystalline tungsten carbide was synthesised in a fashion similar to the temperature-programmed reaction as described in [20]. XC72R carbon (Cabot Corp., BET surface area: 237 $m^2\,g^{-1}$) was added to an aqueous solution of ammonium paratungstate (99%, Riedel-de Haen) in nitric acid (analytical grade) of pH 4 using molar quantities designed to satisfy the stoichiometries of reactions (1) and (2) as follows:

$$WO_3 + 4C \rightarrow WC + 3CO \quad (1)$$

$$2WO_3 + 7C \rightarrow W_2C + 6CO \quad (2)$$

These mixtures were prepared separately and were stirred for 48 h at 70 °C to effect complete wetting of the carbon and impregnation of tungstate ions. The water was then evaporated on a hotplate at 100 °C to ensure fast solvent evaporation and precipitation of small crystals from the aqueous solutions. The powder formed was heated on a hotplate at *ca*. 120 °C overnight, then transferred to a silica furnace boat and placed in a 9-kW furnace. The furnace was deaerated with ultra high purity argon for 1 h at 65 °C. The temperature was then increased to the reaction temperature using a temperature-programmed procedure. The precursors were heated under Ar from 65 to 1300 °C at a ramp rate of 5 °C min^{-1}. The furnace temperature was maintained at 1300 °C for 7 h before cooling to the initial temperature at the same ramp rate. The powder WC and W_2C samples formed were weighed to determine the reaction yield. The yield of WC was >90%. The yield for the W_2C synthesis was less than this, at just 43%, because of the tendency for the reaction to go to completion by forming WC and W.

To synthesise a WC electrocatalytic material containing silver, Ag was precipitated in glycerol in the presence of nanocrystalline WC to form a binary powder. The silver precipitation was carried out according to the procedure in [21]. Silver nitrate (analytical grade) was used as the precursor. A pre-determined amount of the salt, calculated to form 10 wt% Ag in the final catalytic material, was added to a large molar excess of glycerol (analytical grade). The suspension was heated whilst stirring on a hot plate. Upon dissolution of the silver nitrate, nanocrystalline WC (as synthesised above) was added to yield 90 wt% WC, 10 wt% Ag in the final composition. The reaction temperature of 150 °C was measured using a thermometer submerged in the mixture. This temperature was maintained for 2 h to allow the reduction to go to completion before cooling slowly to room temperature. The suspension was then filtered using Whatman filter papers. The filtrate was washed six times with ethanol before overnight drying at 200 °C.

2.2. X-ray diffraction analysis

X-ray diffraction (XRD) analyses of WC, W_2C and WC/Ag were carried out using a Philips PW 1830 generator in conjunction with a Philips C-Tech Cu LFF X-ray diffraction tube. Cu Kα radiation at λ = 1.5405 Å was generated at a voltage of 40 kV and current of 40 mA. The X-ray diffractograms were obtained for 2θ values from 10° to 110° with a step size of 0.05°. Data were collected and analysed using X'ert PRO software.

2.3. Scanning electron microscopy

The powder samples were studied by scanning electron microscopy (SEM) in a field-emission-gun JEOL 6340 microscope. Using secondary electron imaging (SEI), features as small as 5–10 nm are visible.

2.4. Electrode fabrication procedure

Nafion®-bound particulate disc electrodes were fabricated to perform electrochemical testing of the materials. Nafion 117 solution containing 5 wt% Nafion polymer was added to 0.9 g of the synthesised electrocatalysts to provide 20 wt% binder, a system reported to give the optimal Nafion-to-electrocatalyst ratio [22]. The suspension was then sonicated for 15 min and the solvent gently evaporated for a further 15 min until a suitably viscous ink was formed. The electrocatalyst ink was then applied to a 25-mm Toray carbon paper (TGHP-090) disc, wet-proofed with 20 wt% polytetrafluoroethene (PTFE). The disc electrode was dried at 80 °C on a hot plate for 60 min. The electrode was then pressed at the optimal pressure of 100 bar for 5 min [23].

2.5. Electrochemical procedure

Electrodes were tested for corrosion and for electrocatalytic activity potentiostatically. The electrochemical cell consisting of several interconnected modules is shown schematically in Fig. 1. A PTFE counter electrode compartment containing a gold foil counter electrode was fitted to one end of the cell. This was

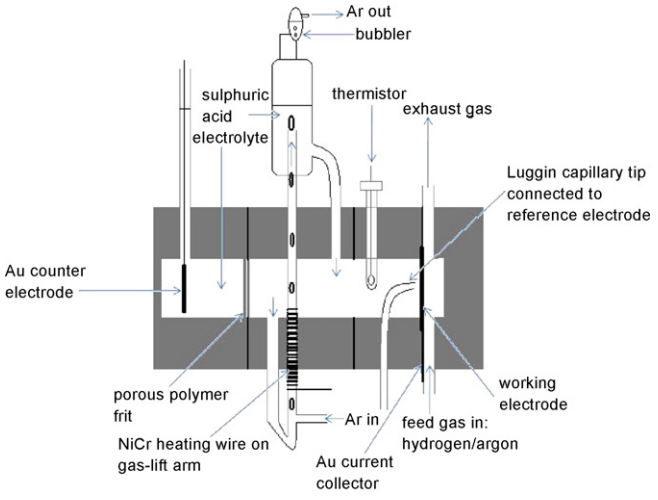

Fig. 1. Schematic of the electrochemical cell.

bolted to the second compartment which contained the electrolyte as well as a gas-lift pump. The electrolyte was heated electrically using a heater mounted onto the gas-lift pump, controlled by an electronically read thermistor which was mounted in the electrolyte compartment. The electrolyte compartment also contained a Luggin capillary probe made from polymethylmethacrylate. The third compartment contained the working electrode which was of 2.15 cm^2 exposed surface area. The current was collected using a Au foil which separated the two compartments. A PTFE gas compartment was attached to the end to permit hydrogen and argon feed, as well as gas exhaust. The reference electrode was mercury/mercurous sulphate/saturated K_2SO_4 (abbreviated to MMS), mounted in a side arm and connected via an electrolyte-filled tube to the Luggin capillary. The MMS reference potential was calibrated against a saturated calomel electrode (SCE) and found to be +0.422 V (SCE), equivalent to +0.666 V (SHE). A microporous borosilicate glass frit was used to separate the counter electrode compartment from the rest of the cell. This prevented gas generated at the counter electrode from reaching the working electrode, whilst still maintaining good electrolytic contact throughout the cell. The temperature in the cell was kept constant at 65 °C for all experiments presented. The heater was a home-made nichrome-heating element fitted to an arm of the gas-lift cell. The gas-lift cell was used to deaerate the electrolyte with pure Ar prior to and during fuel testing and corrosion testing experiments.

Because the test materials are not noble and depend on passivity against corrosion for their stability in the sulphuric acid electrolytes, corrosion and passivation tests were performed in the working cell prior to admission of the hydrogen feed gas. These corrosion/passivation tests were performed potentiostatically with pure argon flowing through the gas compartment. Following corrosion testing, the electrodes were examined for their electrocatalytic activity towards the oxidation of hydrogen gas as well as for the cathodic evolution of hydrogen.

The test electrode was placed in the cell with the electrocatalyst facing the electrolyte. The cell was filled with 1.5 M H_2SO_4 (analytical grade reagent) and twice-distilled water. High purity argon was bubbled through the gas-lift pump for an hour before and then during testing: this removed residual oxygen from the electrolyte and distributed heat evenly within the cell. Potentiostatic testing was then carried out to obtain quasi-steady-state currents. Potentiostatic transients at incremental intervals of 50 or 100 mV covering the range of −0.65 to −0.35 V (MMS) were imposed. Typically, the corrosion rate was determined during the first 400 s of each potentiostatic transient using Ar as the feed gas. At 400 s, the Ar feed gas was stopped and H_2 fuel supplied to the gas compartment at ambient pressure to determine the hydrogen oxidation activity of the electrode. The time for a steady-state hydrogen oxidation current to be established varied amongst electrodes with the consequence that the hydrogen feed gas was supplied for periods between 200 and 500 s. Finally the H_2 feed gas was shut off and Ar was again fed through the gas compartment. In this stage, the current was allowed to decline to (or towards) the corrosion baseline current before potential control was terminated. Each transient thereby gave a corrosion current and a catalysis current recorded as a function of time over a total of *ca.* 1200 s. The current was recorded using a data acquisition rate of 1 Hz. The procedure was repeated for different applied potentials.

We also determined the electrocatalytic activity towards the cathodic evolution of hydrogen using potentiostatic transients between −0.7 and −0.8 V (MMS) at 25 mV increments. These were performed on the electrode immediately after testing for the anodic corrosion and hydrogen oxidation activity. The potentiostatic cathodic transients were carried out for 40–100 s at each potential using the same data acquisition rate to determine a quasi-steady-state current density for hydrogen evolution. The shorter time used for these cathodic transients was to minimise the risk of mechanical microscopic damage to the electrode potentially arising from the gas evolution process. This possible form of damage has not been assessed. Note that current densities presented throughout this paper are normalised with respect to the projected surface area of the electrode (2.15 cm^2), and not the true surface area of the catalyst, which was not measured.

3. Results

3.1. XRD characterisation

The XRD pattern of the synthesised WC is shown in Fig. 2a. It reveals peaks corresponding to hexagonal tungsten carbide, WC, confirming the synthesis. Also visible in the diffraction patterns are very low intensity peaks due to the lower carbide, W_2C as well as metallic tungsten. The amounts of W and W_2C in these samples were found to be <2 mol% by X'pert PRO software analysis, confirming that we had synthesised fairly pure WC. The W_2C and W formed are the products of incomplete thermal reduction during the reaction. No carbon peaks were observed at low Bragg angles indicating that all the graphitic carbon had been consumed during the carburisation reaction.

The XRD pattern in Fig. 2b represents the product of the combined synthesis of WC and Ag. This diffraction pattern shows peaks corresponding to hexagonal WC and to cubic Ag only. No other peaks corresponding to lower oxidation states of tungsten (W or W_2C) was observed; neither was any excess carbon present.

The synthesis of nanocrystalline W_2C was not quite as clear, as shown in the diffraction pattern in Fig. 2c. This synthesis yielded a mixed composition containing WC, W_2C and metallic W, whose diffraction peaks are identified in Fig. 2c. Semi-quantitative analysis using X'pert PRO software showed concentrations of WC, W_2C and W in this sample to be 50, 43 and 7 mol%, respectively. This shows control of the synthesis was not perfect with respect to W_2C which was targeted. Simply controlling the mole ratios of the starting materials is clearly insufficient for this. It is clear that the reaction carried out under the conditions described above displays a tendency to go to completion by forming WC. This then leaves a deficiency of carbon which can only partially reduce the tungsten oxide to W_2C and W. This may well proceed by partial disproportionate of the W_2C to WC and W. However, the synthesis gave sufficient W_2C to allow determination of the corrosion rate and

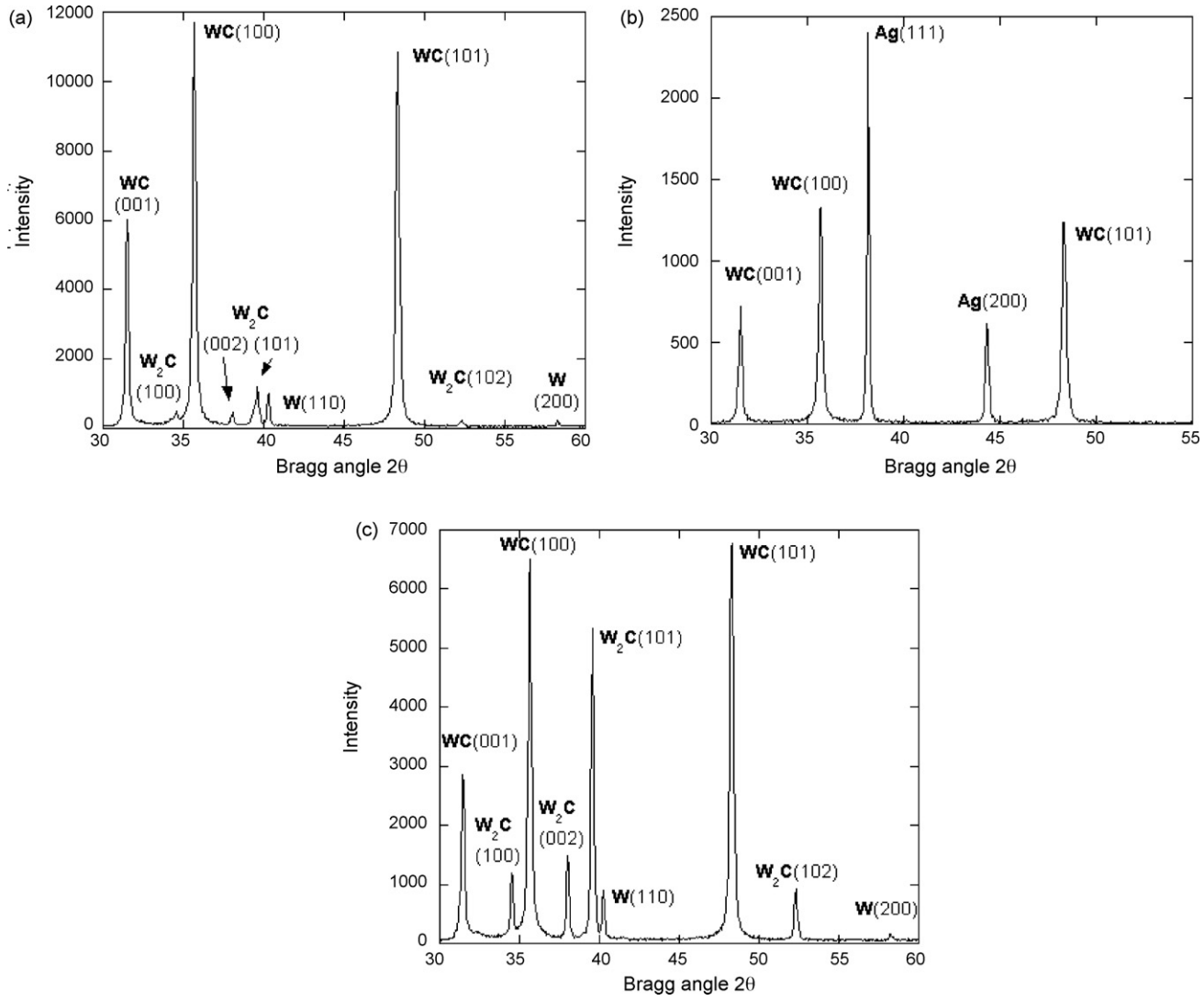

Fig. 2. (a) XRD pattern of synthesised nanocrystalline WC. (b) XRD pattern of synthesised WC/Ag. (c) XRD pattern of synthesised nanocrystalline W_2C/WC.

electrocatalytic activity of the material in comparison with the WC stoichiometry.

3.2. SEM analysis

An SEM image of the synthesised pure WC is shown in Fig. 3a. It reveals a faceted nanocrystalline structure with a fairly uniform crystal size of diameter between 50 and 200 nm. They are therefore borderline when categorized as nanoparticles, normally defined at <100 nm in at least one dimension. Sintering between adjacent particles is visible and results in a porous network running amongst the crystals. Sintering amongst particles occurs because of the high reaction temperature.

Fig. 3b shows a typical WC/Ag microstructure from the codeposited materials. In this micrograph, a single large Ag crystal (0.5–2 μm diameter) is observed, which is decorated with WC nanocrystals. These large Ag crystals were typical of this synthesis, and were dispersed throughout the WC material.

Fig. 3c shows the crystals formed during synthesis of W_2C. The material was in fact a mixture of W_2C/WC as shown in Fig. 2c. Nevertheless, the crystals of W_2C appeared very similar in shape and particle size to the WC shown in Fig. 3a. Fig. 3c is shown at a lower magnification in order to depict the uniformity of the fine material dimensions over a larger area.

3.3. Electrochemical testing

Fig. 4 shows a graph of current as a function of time for each of the three materials polarised at −0.4 V (MMS) at the working temperature of 65 °C. The experiment for each electrode was performed by first passing Ar through the gas compartment to measure passivation against corrosion, then replacing the Ar with hydrogen gas to measure the anodic electrocatalytic activity, and finally replacing the H_2 by Ar again. The arrows marked in the diagram show where the gas flow was changed from Ar to H_2 and back again. (There is a finite time between changing the gas and observing the current response to that change, which describes the time taken for the new gas to flow through the delivery pipework to the electrode surface.) All three materials show the same type of behaviour. All passivate (against corro-

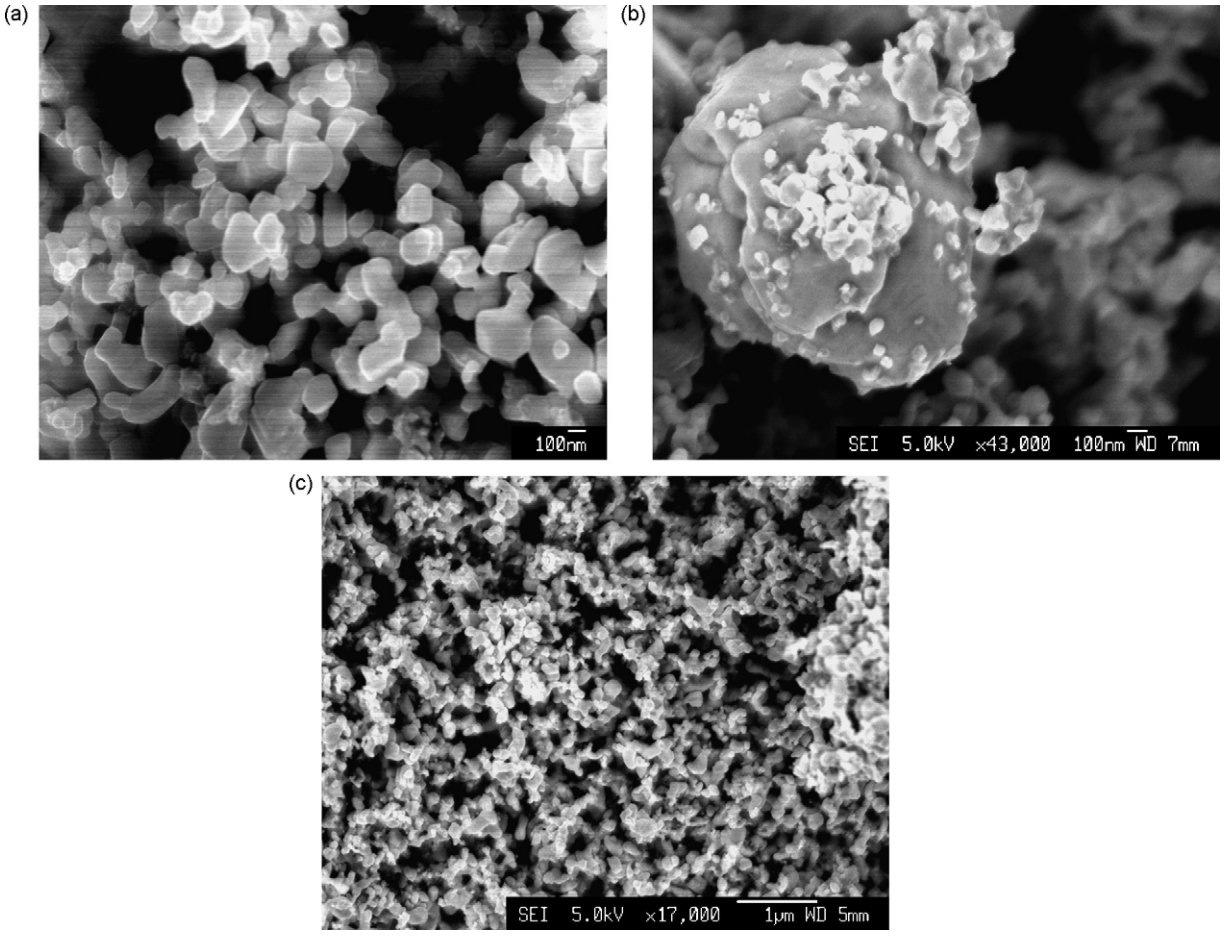

Fig. 3. (a) SEM image of nanocrystalline WC. (b) SEM image of a silver crystal decorated with WC nanocrystals typical of the WC/Ag electrocatalyst structure. (c) SEM image of synthesised nanocrystalline W_2C/WC.

sion) initially as seen by the rapidly declining current under the inert gas. Switching the feed gas from argon to hydrogen results in a sharp anodic rise in current by 11.5, 31 and 38 mA cm^{-2} for W_2C/WC, WC and WC/Ag electrodes, respectively. Removing the fuel and reverting back to the Ar feed gas engenders a sudden decline in anodic current back towards the passive baseline. Admission of the hydrogen feed shows thereby that all three materials are electrocatalytically active towards the anodic oxidation of hydrogen, with the highest current density observed on the WC/Ag electrode and the lowest current density on the W_2C/WC electrode (the current trace for the WC/Ag electrode did not return to the baseline corrosion current because of residual hydrogen leaking into the argon line and giving rise to small residual hydrogen oxidation currents: this does not however, affect the results).

Fig. 4 shows the polarisation data accumulated from the hydrogen current transients performed on the WC, W_2C/WC and WC/Ag electrodes. Fig. 5a shows the data using a linear current scale and the same data are shown in logarithmic form in Fig. 5b. Both the anodic hydrogen oxidation currents and those due to cathodic evolution of hydrogen are plotted. The WC/Ag delivers approximately 25% more anodic current during the oxidation of hydrogen than does the WC electrode alone. The WC electrocatalyst delivers about twice the hydrogen oxidation current than the W_2C/WC electrode. It is apparent from this graph, as in Fig. 4, that the WC/Ag electrode is a better electrocatalyst than WC alone, possible causes for which are discussed below. The WC electrode is in turn a better electrocatalyst than the W_2C/WC electrode. In the cathodic regime, a similar trend is seen. For example, at −0.8 V (MMS), representing a cathodic hydrogen overpotential of 0.133 V, the WC electrode gives a peak current density of 47 mA cm^{-2} whilst the WC/Ag electrode yields 86 mA cm^{-2}, almost twice as large. The W_2C/WC electrode is again the least active of the three catalytic materials. We deduce that W_2C possesses an inherently lower electrocatalytic activity than WC, both anodically and cathodically. We show below that the W_2C electrode corrodes at the highest rate of the three materials, which must itself be intrinsically detrimental to the electrocatalytic activity of the surface.

It is seen in Fig. 5b that the cathodic evolution of hydrogen follows approximately the Tafel relationship: the cathodic Tafel slopes are listed in Table 1. The anodic branches can also be fitted to the Tafel equation, although Fig. 5b shows that these anodic lines are in fact curved.

These materials are base materials. The anodic electrocatalysis reactions are carried out over a potential range where tungsten is thermodynamically unstable [17]. They therefore depend for their stability in the electrolyte on a state of passivity against

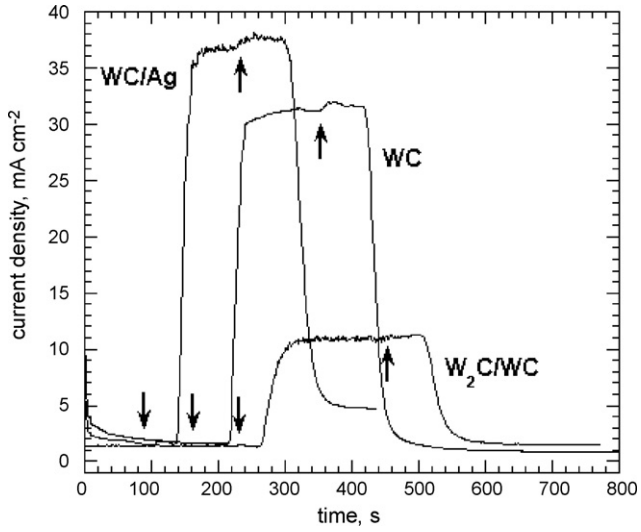

Fig. 4. Current density–time plots for the three catalysts showing initial passivation under argon flow followed by admission of hydrogen followed by removal of hydrogen. The three downward pointing arrows mark the point where the argon flow is terminated and hydrogen is admitted for each electrocatalyst in the order WC/Ag, WC and W_2C/WC, respectively. The upward pointing arrows mark the corresponding points for the removal of the hydrogen supply and readmission of argon. The delay observed in each case between the change of gas and the change of current is due to the length of gas piping between the supply and the electrode.

Table 1
Cathodic Tafel slopes (b_c) and exchange current densities (i_0) for the hydrogen reaction on the catalysts as shown

Catalyst	$-b_c$ (mV dec^{-1})	i_0 (mA cm^{-2})
WC	96	1.8
WC/Ag	70	1.1
W_2C/WC	75	0.68

The exchange current densities were obtained by extrapolation of the cathodic Tafel line to the hydrogen equilibrium potential, −0.667 V (MMS). The surface area used was the projected surface area of the entire electrode.

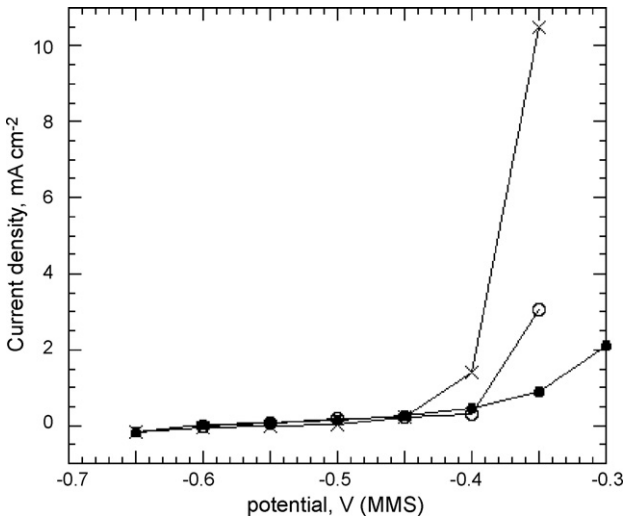

Fig. 6. Current density, measured after *ca*. 300 s due to corrosion of the electrocatalysts: WC (●), WC/Ag (◯), and W_2C/WC (×). Electrolyte: 1.5 M H_2SO_4; temperature: 65 °C; measured under argon. Note that these are not true steady-state current densities but are still declining at the point of measurement.

corrosion. We show in Fig. 6 corrosion currents measured potentiostatically (not at open circuit) for the three electrocatalysts across the range of potentials suitable for fuel cell hydrogen anodes, as well as some more positive potential. The currents at each potential are not yet steady state at the end of the time plots, as shown in Fig. 7. Nevertheless, they are already low corrosion currents: below 300 μA cm^{-2} observed up to −0.45 V (MMS) on all three electrodes, and still declining at the end of each of the measurements. For potentials ≥−0.400 V (MMS) there is a significant increase in the corrosion current with further increase in potential, particularly for the W_2C/WC electrode. This is due to the fact that both tungsten carbides undergo a breakdown of their passivity and dissolution of the tungsten into the sulphuric acid electrolyte. Although all three catalysts do this, the fastest

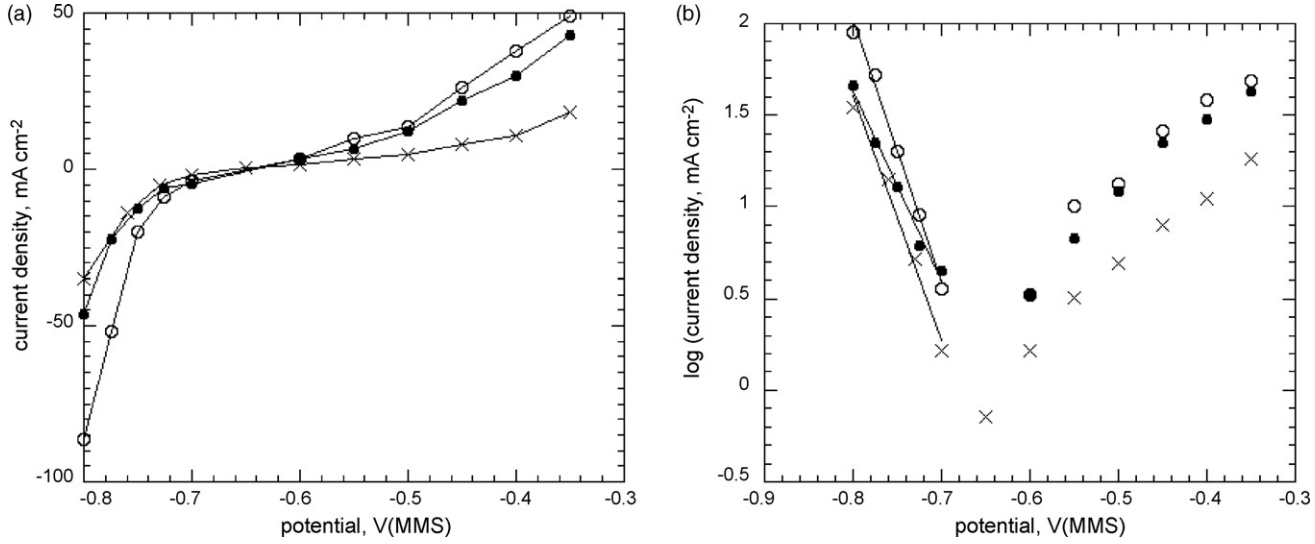

Fig. 5. (a) Current density vs. potential plots for anodic hydrogen oxidation (positive current) and cathodic hydrogen evolution (negative current) for the three electrocatalysts WC (●), WC/Ag (◯), and W_2C/WC (×) in 1.5 M H_2SO_4 at 65 °C. (b) The same as Fig. 5a with the current density on a logarithmic scale. The cathodic data have been linearly regressed to show the cathodic Tafel lines.

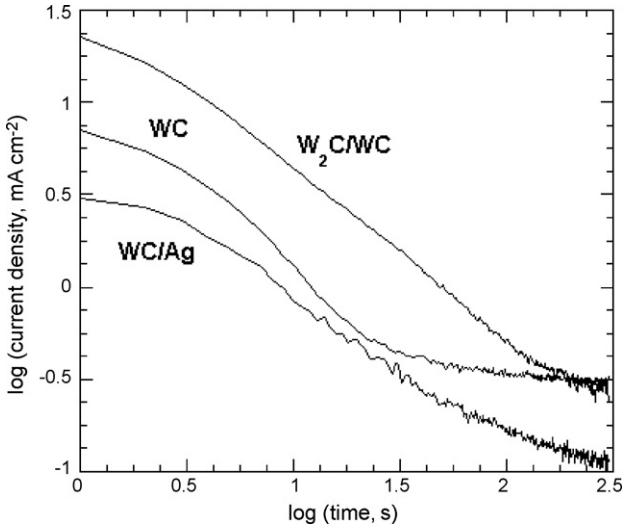

Fig. 7. Potentiostatic current transients presented on logarithmic axes for the three electrocatalysts indicated at −0.45 V (MMS) in 1.5 M H_2SO_4, temperature: 65 °C. These transients were measured under argon and described passivation of the materials.

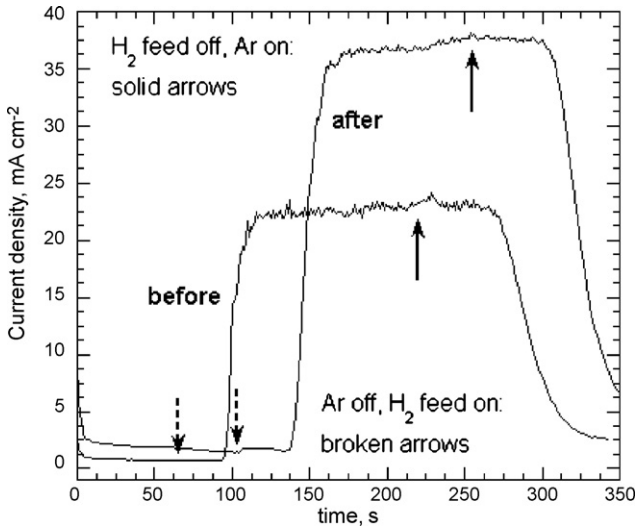

Fig. 8. Potentiostatic current transients showing passivation of WC/Ag and hydrogen oxidation showing the effect of prior potential cycling. The catalyst passivates initially under argon. The hydrogen feed is initiated at the downward pointing arrows (broken) and terminated at the upward pointing arrows (solid). The transient labelled before is the initial run at −0.4 V (MMS). The transient labelled after was achieved also −0.4 V (MMS) but after the same electrode had been anodically treated up to −0.3 V (MMS). The graph shows acceleration of the hydrogen reaction due to high potential treatment.

increase in corrosion rate by far is that of the W_2C/WC electrode. The WC/Ag and WC corrosion currents increase above −0.4 V (MMS) but more slowly. Note that there is an increased corrosion rate for WC/Ag observed at −0.35 V (MMS) in comparison with WC: this is attributed to the onset of the anodic dissolution of silver (at 25 °C the standard electrode potential for the Ag^+/Ag reaction is +0.122 V (MMS) [17]).

It is important to note here too, that although the corrosion currents continue to decline with time, beyond the recording period, this decline does not affect the anodic electrocatalytic activity towards hydrogen oxidation. As shown in Fig. 4, the hydrogen oxidation currents reach a steady state remarkably quickly. Indeed, detailed inspection of the hydrogen plateau current in each case shows that the current in fact increases very slowly with time. This has been observed with all the current transients measured in this work, although the effect is small.

Fig. 7 illustrates the declining corrosion currents as a function of time for the three electrocatalytic materials. The WC/Ag electrode shows the best passivation characteristics with currents declining steadily. The WC and W_2C/WC corrosion currents continue to decline although a slower rate of current decay is noted. We do not yet have data that show the complete steady-state corrosion currents: however, they are clearly much lower than those presented here.

At higher potentials (>−0.4 V (MMS)), the silver component of the WC/Ag electrode is able to dissolve anodically, as noted above. This means that after a full range of potential has been covered in the anodic regime, some silver would have dissolved out anodically at the higher potentials used, and this would be capable of cathodic deposition on the surface of the working electrode when the potential is reduced again. We show the effects of this as follows. At the conclusion of a run comprising a full range of anodic potentials up to −0.3 V (MMS) (in 50 mV intervals) the potential was returned to −0.4 V (MMS) and tested again. Fig. 8 shows the electrocatalytic effect consequent upon this procedure for the WC/Ag electrode. The electrocatalytic activity towards hydrogen oxidation has increased, rising from 23 mA cm^{-2} before the high-potential treatment to 38 mA cm^{-2} afterwards. Bearing in mind that these measurements were carried out on the same electrode, this is a true rise in electrocatalytic activity. This interesting observation is presented because not only does it show that reorganisation of the Ag deposit can improve the performance of these catalysts, but also shown is the fact that the WC, which would also have undergone significant corrosion and passivation at the higher potentials, still remains electrocatalytically active towards the hydrogen oxidation reaction. Clearly the passive WC surface remains intact during this high potential processing and there must also be a further effect due to Ag. We ascribe the silver effect to the following. Initially the Ag particles within the material are quite large (*ca.* 500 nm diameter, see Fig. 3b). Increasing the potential leads to anodic dissolution of the silver. Subsequent application of a low potential causes Ag^+ to be cathodically redeposited by reduction onto the WC nanoparticles, decorating the surface of the WC with silver. The silver is then dispersed more effectively within the electrode and in doing so increases the electrocatalytic activity of the material. Fig. 8 shows a 16 mA cm^{-2} increase in the hydrogen oxidation current after potential cycling. This is attributed to the dispersion of silver across the carbide surface giving rise to the electrocatalytic synergistic phenomenon. We note that we tested pure silver for electrocatalytic activity towards hydrogen oxidation, and found no evidence of electrocatalysis. The synergistic action between the Ag and the WC component described above is thereby a true synergy.

A similar effect of silver by Walters et al. [18] was proposed to improve the hydrogen evolution catalysis on tantalum by low coverage electrodeposition of silver onto the tantalum surface.

This phenomenon is however unlikely to have the same origin as the observations reported here, since in the absence of the silver, tantalum forms an electron-insulating passive oxide film which would certainly retard hydrogen evolution.

4. Discussion

This method of synthesising tungsten carbides of nanocrystalline dimensions obviates the simultaneous production of carbon. In previous methods, where tungsten carbides (as well as other carbides) were produced by gas-phase reduction of W(VI) using methane/hydrogen mixtures, much carbon was also deposited [8–11], and this was detected by XRD. The advantage of this high-temperature solid-state synthesis is therefore the production of clean W_2C/WC surfaces, without residual carbon coated on the surface: no carbon peaks were observed in the XRD patterns in Fig. 2. None would be expected either, since the synthesis employs only sufficient carbon to satisfy the stoichiometries of the reaction. Since there are no residual tungsten oxide peaks from the precursor in the XRD patterns, all the tungsten has been reduced, and only the incorporated carbon could do that. Carbon residues are commonly found when carburising in a carbonaceous gas [24]. For effective electrocatalysis of the hydrogen oxidation reaction, it is likely that the material must have electrocatalytically active sites and thus a residue-free surface is desirable. In the present synthesis, the tungsten oxide precursor is precipitated on the surface of high-surface-area carbon. Provided the reaction is carried out stoichiometrically, there can be no residual carbon, and no mechanism for its reformation. The hydrogen oxidation current densities presented above are higher than those achieved previously [5], but not very much so. The improved current densities for hydrogen oxidation of WC observed here can arise either from the fact that the surfaces are cleaner, with less elemental carbon, or from the fact that the particle size is smaller, probably both.

There are two possible origins for the passivity of carbides against corrosion in aqueous solution. The system can passivate by formation of a tungsten oxide film, as expected from metallic tungsten [17], with the carbon component residual to that. Alternatively, some dissolution of tungsten from the surface of the carbide may leave the surface rich in carbon, giving passivation by a carbon layer. We propose here, that the carbon component itself acts as a passivating agent together with a WO_3 film. The reason for this arises from the comparison in behaviour between the two carbides, WC and W_2C. Noted above is the fact that the W_2C phase is less passive than the WC phase. At higher potentials, the corrosion currents of the W_2C phase are very much higher than those of WC. For example, at -0.35 V (MMS) WC shows a corrosion rate of 3 mA cm^{-2} whereas W_2C shows 10.5 mA cm^{-2} at the same potential. Note too in this comparison, that only about half of the W_2C/WC electrode is in fact W_2C, so the true comparative corrosion current density for the W_2C phase must be even higher. This implies that the lower carbide (W_2C) is less passive than WC, and the phenomenon is explicable only by invoking that at least some of the passivity is imparted by the carbon component. However, within this argument lies the fact that the greater corrosion currents observed for the W_2C phase are those observed where the carbide indeed shows transpassive dissolution, i.e. at potentials >-0.45 V (MMS). We have not observed greater corrosion current densities in the truly passive region, where $E \leq -0.45$ V (MMS). In this region both carbides show a very high degree of passivity, and we are unable to distinguish their relative passive current densities. We must nevertheless deduce that, at least at the higher potentials, the surface enriches in carbon, which aids passivity. It is therefore likely to be true also at the lower potentials. (If passivation were by a film of WO_3 alone, we would expect the lower carbide to be more passive than the WC phase since the higher carbon content of the latter would be expected to disrupt the passive state more than that with the lower carbide, opposite to the observations shown above).

Turning now to the electrocatalysis, we note that the anodic oxidation of hydrogen on the W_2C phase is slower than that on the WC phase at all potentials investigated, as borne out by the Tafel plots of Fig. 5b. Moreover, the plots for all three electrocatalysts are parallel, both in the anodic direction and (separately) in the cathodic direction. This implies that the W_2C phase is truly a poorer electrocatalyst, independently of whether it is in the fully passive state at lower potentials, or whether it is in the transpassive region, at potentials >-0.45 V (MMS). The carbon component of the surface is itself therefore important to the electrocatalysis. This argument is firmly based in Fig. 5b. The anodic branch of this Tafel plot is a difficult one to model because it depends on how well the gas is supplied to, and distributed over the electrode/electrolyte interface. This problem besets all gas-fed fuel electrodes, because it requires the creation of the three-phase interface. We note that the gradient of the anodic branch of Fig. 5b were it expressed as a Tafel slope, would be much greater than that of the cathodic branch. However, in the cathodic region of Fig. 5b, the hydrogen evolution domain, the entire electrode/electrolyte interface is active, and gas can be, and is generated everywhere. The Tafel lines here can be regarded as true Tafel lines, and the comparison between the three electrocatalysts drawn. It is clear here too, that the W_2C phase is a poorer electrocatalyst than the WC phase. It therefore appears that the carbon component is necessary to allow better electrocatalyst function. The oxidised surface of the tungsten as well as the carbon component are thus both necessary for this electrocatalysis. The list of Tafel parameters for each electrocatalyst is shown in Table 1. Note that although the Tafel lines themselves show clear differences in electrocatalytic activity, it is not possible to draw the same information from the exchange current densities: these were obtained by extrapolation to the hydrogen equilibrium potential and any scatter in the measured cathodic Tafel slopes are magnified in that extrapolation. Nevertheless, exchange current densities of around 1 mA cm^{-2} of projected surface area for all the electrocatalysts reported above are apparent.

It is important also to point out the following. In Fig. 4, at the point where the hydrogen fuel is injected into the cell, the hydrogen oxidation current reaches an approximate steady state quite quickly: the rise time of the current transient is a maximum of *ca*. 30 s. For the period of the hydrogen test, the current density

then actually continues to rise, albeit at a very slow rate. (The apparent plateau with time in hydrogen oxidation current shows a small positive gradient, seen by inspection.) This has been observed consistently with all three electrocatalysts, (as well as with results not reported here). The important point arising from this observation, is that during this period of time, the corrosion current of the electrocatalysts is still declining as the catalyst passivates, but the electrocatalysis current increases (slightly). It appears then, that as passivation (against corrosion) continues to occur, in this particular case including the enrichment of carbon on the surface (described above), the hydrogen oxidation reaction is enhanced. This again, points to the carbon component being critical to the electrocatalysis.

The role of silver is more difficult to explain. Silver catalyses both the anodic and cathodic hydrogen reactions, but is itself a very poor electrocatalyst for hydrogen oxidation. Its role is therefore in synergy with that of the WC component. It is seen further, that by redistributing the silver, the activity can be enhanced further, shown in Fig. 8. We believe that the redistribution of the Ag takes place as follows. During testing at higher potential the silver becomes more dispersed because of its anodic dissolution in the electrolyte: reducing the potential subsequently then causes cathodic reduction of the dissolved silver back onto the WC. The implication is that Ag deposited over the WC, or perhaps at the interface between the WC and Ag phases, provides a higher degree of activity: the effect on both anodic and cathodic hydrogen reactions, which is quite reproducible, is however, fairly small. The effect of Ag could also be electrical. By dispersing the metallic Ag throughout the catalyst, better electronic contact amongst particles could be achieved. Although this could not affect the ohmic potential drop significantly, it could bring more catalyst particles in the electrode into a working condition. Any catalyst particles which are not in electronic contact with other particles cannot function as electrocatalyst. Some electrically detached particles occur during fabrication of the electrode, and the presence of silver must simply improve that contact and reduce the fraction of isolated crystals. The effect remains to be proven.

The quest continues for electrocatalysts made only from base materials that could be capable of use in fuel cells. Tungsten carbide is such a non-noble material which passivates well against corrosion in acidic electrolytes. We note however, that the carbide is prone to corrosion at higher potentials [17] and for this reason, could not be used as a cathode electrocatalyst for reduction of oxygen. Silver too, corrodes at high potentials in acidic solutions [17].

We have tested these WC based for periods a little over an hour and found no degradation in performance [5]. The behaviour over much longer periods has yet to be examined.

The performance of these WC-based electrodes is considerably lower than that of similar Pt electrodes [25], but for a platinum-free system is significant.

5. Conclusions

1. Nanocrystalline WC and W_2C, of particle diameter between 50 and 200 nm, can be synthesised by solid-state thermal reaction between WO_3 precipitated onto high-surface-area XC72R carbon. The carbides formed possess clean surfaces with no detectable carbon deposits.
2. The synthesised WC forms an effective hydrogen oxidation anode as well as a hydrogen evolution cathode. This is attributed to the intrinsic electrocatalytic activity of WC, the fine particle size of the material and the clean carbide surfaces formed.
3. W_2C is a less electrocatalytically active material than WC as well as being less passive in sulphuric acid electrolytes.
4. The presence of surface carbon which accumulates on the carbide surface by dint of tungsten dissolution during passivation, is a necessary component for this electrocatalyst.
5. Decreased particle size leads to increased corrosion currents and reduces the applicable electrochemical window of WC to an anodic hydrogen overpotential of 0.25 V in hot sulphuric acid.
6. An electrocatalytic synergistic effect occurs between silver electrodeposited onto the WC surface. This gives rise to improved electrocatalytic performance of the material as a hydrogen oxidation electrocatalyst as well as enhancing the rate of cathodic evolution of hydrogen.

Acknowledgements

We are grateful to the EPSRC for financial support of this research programme by way of research studentships. The programme is partially supported by the New Zealand Foundation for Research, Science and Technology, to whom we are also grateful under contract no. C08X0409.

References

[1] G.J.K. Acres, J.C. Frost, G.A. Hards, R.J. Poter, T.R. Ralph, D. Thompsett, G.T. Burstein, G.J. Hutchings, Catal. Today 38 (1997) 393.
[2] J. Yu, T. Matsuura, Y. Yoshikawa, M. Nazrul Islam, M. Hori, Electrochem. Solid-State Lett. 8 (2005) A156–A158.
[3] R.B. Levy, M. Boudart, Science 181 (1973) 547.
[4] L.H. Bennett, J.R. Cuthill, A.J. McAlister, N.E. Erickson, R.E. Watson, Science New Series 187 (1975) 858–859.
[5] D.R. McIntyre, G.T. Burstein, A. Vossen, J. Power Sources 107 (2002) 67–73.
[6] E. Salje, K. Viswanthan, Acta Cryst. A31 (1975) 356.
[7] M. Nagai, M. Yoshida, H. Tominaga, Electrochim. Acta 52 (2007) 5430–5436.
[8] G.T. Burstein, C.J. Barnett, A.R. Kucernak, K.R. Williams, J. Electrochem. Soc. 143 (1996) L139.
[9] G.T. Burstein, C.J. Barnett, A.R. Kucernak, K.R. Williams, Catal. Today 38 (1997) 425.
[10] C.J. Barnett, G.T. Burstein, A.R. Kucernak, K.R. Williams, Electrochim. Acta 42 (1997) 2381–2388.
[11] D.R. McIntryre, A. Vossen, J.R. Wilde, G.T. Burstein, J. Power Sources 108 (2002) 1–7.
[12] K. Sawai, N. Suzuki, J. Electrochem. Soc. 151 (2004) A682–A688.
[13] S.Lj. Gojkovic, S. Gupta, R.F. Savinell, J. Electroanal. Chem. 462 (1999) 63–72.
[14] H. Khong, H. Zhang, G. Liu, Y. Liang, J. Hu, B. Yi, Electrochem. Commun. 8 (2006) 707–712.
[15] H. Khong, H. Zhang, Y. Liang, J. Zhang, M. Wang, X. Wang, J. Power Sources 164 (2007) 572–577.
[16] F.W. Clinard, C.P. Kempter, J. Less-Common Met. 15 (1968) 59–73.

[17] M. Pourbaix, Atlas of Electrochemical Equilibria in Aqueous Solutions, Pergamon Press, Oxford, 1966, 280, 393 pp.
[18] M.J. Walters, K.A. Assiongbon, D.R. Marr, B.T. Shepardson, D. Roy, Int. J. Hydrogen Energ. 28 (2003) 285–295.
[19] M. Meng, P.K. Shen, Electrochem. Commun. 8 (2006) 588–594.
[20] N. Keller, B. Pietruszka, V. Keller, Mater. Lett. 60 (2006) 1774–1777.
[21] A. Sinha, B.P. Sharma, Bull. Mater. Sci. 28 (2005) 213–217.
[22] G. Sasikumar, J.W. Ihm, H. Ryu, Electrochim. Acta 50 (2004) 601–605.
[23] B. Nakrumpai, K. Pruksathorn, P. Piusomboon, Korean J. Chem. Eng. 23 (2006) 570–575.
[24] J.H. Kim, L.K. Kim, Appl. Catal. A 181 (1999) 103.
[25] A.R. Kucernak, G.T. Burstein, C.J. Burstein, K.R. Williams, J. Appl. Electrochem. 27 (1997) 1304–1306.